

LL-Localizer: A Life-Long Localization System based on Dynamic i-Octree

Xinyi Li¹, Shenghai Yuan², Haoxin Cai¹, Shunan Lu¹, Wenhua Wang¹, Jianqi Liu^{1*}

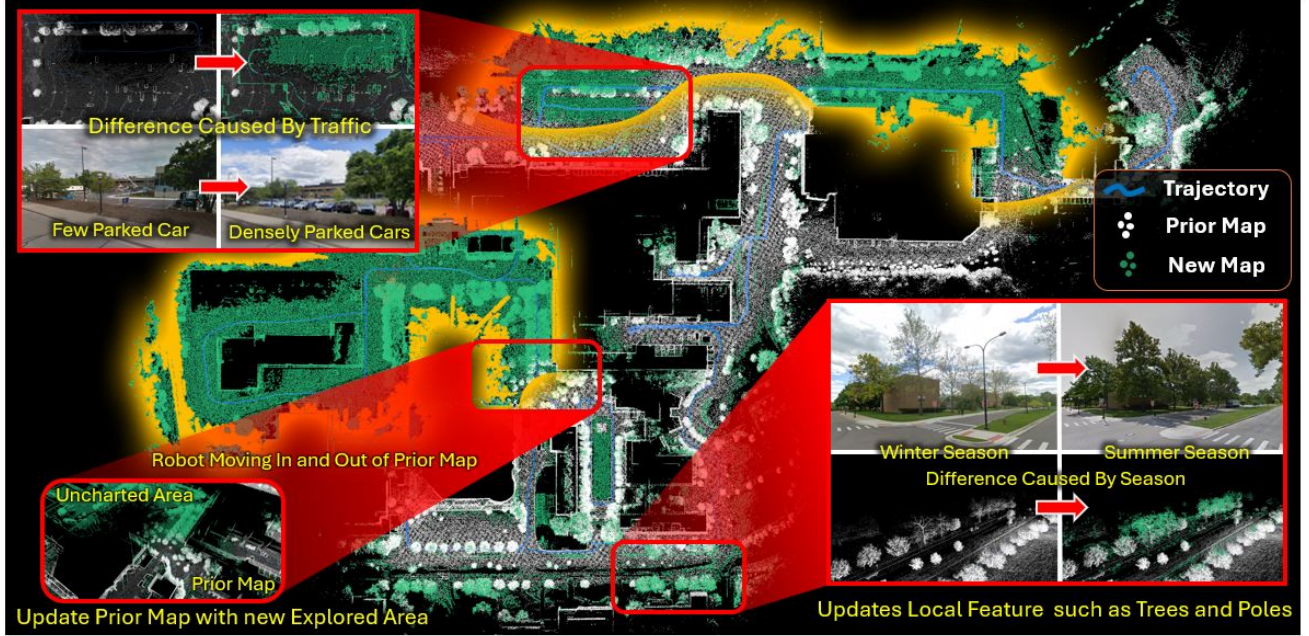


Fig. 1. Motivation for our incremental voxel-based life-long localization approach. The white point cloud denotes the prior map loaded at startup, while the green point cloud highlights incremental updates to accommodate new areas or environmental changes (e.g., traffic, seasons). This functionality is crucial for long-duration service robots.

Abstract—This paper proposes an incremental voxel-based life-long localization method, LL-Localizer, which enables robots to localize robustly and accurately in multi-session mode using prior maps. Meanwhile, considering that it is difficult to be aware of changes in the environment in the prior map and robots may traverse between mapped and unmapped areas during actual operation, we will update the map when needed according to the established strategies through incremental voxel map. Besides, to ensure high performance in real-time and facilitate our map management, we utilize Dynamic i-Octree, an efficient organization of 3D points based on Dynamic Octree to load local map and update the map during the robot's operation. The experiments show that our system can perform stable and accurate localization comparable to state-of-the-art LIO systems. And even if the environment in the prior map changes or the robots traverse between mapped and unmapped areas, our system can still maintain robust and accurate localization without any distinction. Our demo can be found on Bilibili <https://www.bilibili.com/video/BV1faZHYCEkZ> and youtube <https://youtu.be/UWn7RCb9kA8> and the program will be available at <https://github.com/M-Evanovic/LL-Localizer>.

Index Terms—Robotics, Life-long, Localization.

I. INTRODUCTION

LOCALIZATION is a key technology for mobile robots, enabling them to navigate autonomously in diverse environments. Life-long localization utilizes prior maps to achieve localization and map updates across multi-session. While many state-of-the-art LiDAR odometry (LO) and LiDAR-inertial odometry (LIO) systems [1]–[9] perform well in localization and mapping, they are designed more for single-session scenarios rather than multi-session applications. Consequently, their ability to handle spatial and temporal correlations is limited, making it challenging to extend them to life-long localization and mapping mode.

In life-long deployment, prior maps are commonly used for localization. However, even with high-precision prior maps, life-long localization still faces several challenges. Map-based localization methods [10], [11] directly constrain the current pose by aligning the current scan with the prior map. However, if the environment in the prior map changes or the robot enters an area without prior map, pose estimation will become unreliable due to inaccurate or insufficient prior knowledge. Although the Global Navigation Satellite System (GNSS) can directly provide the robot's absolute position, it has an inherent limitation, as GNSS data may be unavailable or unreliable in GNSS-denied environments.

*Corresponding Author. This work was supported in part by the National Science Foundation of China under Grant 62172111, National Joint Fund Key Project (NSFC - Guangdong Joint Fund) under Grant U21A20478.

¹Xinyi Li, Haoxin Cai, Shunan Lu, Wenhua Wang, Jianqi Liu are with School of Computer Science, Guangdong University of Technology, Guangzhou 510006, China. Email: xinyili@mail2.gdut.edu.cn, hxcai@mail2.gdut.edu.cn, shunanlu@mail2.gdut.edu.cn, wenhuawang@mail2.gdut.edu.cn, liujianqi@ieee.org.

²Shenghai Yuan is with Centre for Advanced Robotics Technology Innovation, Nanyang Technological University, Singapore. Email: shyuan@ntu.edu.sg

In practical life-long deployment, robots can enter unknown areas (yellow regions highlighted in Fig. 1) where there is no prior map during autonomous navigation. If the robot fails to recognize that it has entered an unknown area and does not update the surrounding map, localization failure may occur, leading to system failure. Likewise, if environmental changes occur within the prior map region (red box in Fig. 1), point cloud registration may fail, resulting in significant localization errors.

To address these limitations, we propose LL-Localizer, which focuses on tackling life-long localization challenges: even as the robot traverses between mapped and unmapped areas or when the environment within the map changes, it can still maintain robust localization while simultaneously updating the map.

The main contributions in this paper are summarized as follows:

- With the proposed map management approach, the system can autonomously and flexibly switch between map-based localization and SLAM modes during operation, ensuring consistently accurate and robust localization in both mapped and unmapped areas.
- Our local map loading method, built upon the proposed map management approach, enables accurate point cloud registration to ensure robust localization even when environmental changes occur within the prior map. At the same time, our system allows updating the map to reflect these changes.
- We propose Dynamic i-Octree for efficient map management, greatly accelerating local map loading and map updates. This enhancement allows our system to maintain real-time performance even in dense maps.

II. RELATED WORKS

A. LO / LIOs

The Iterative Closest Point (ICP) method introduced by Besl et al. [12] has long served as a fundamental technique for scan registration [13], forming the basis of many LiDAR Odometry (LO) systems. While ICP performs well on dense 3D scans with accurate point correspondences, its strict reliance on exact matches makes it less suitable for sparse point clouds. To address this limitation, Segal et al. proposed the generalized-ICP (G-ICP) algorithm [14], which leverages point-to-plane distances instead of exact matches. Building on this idea, Zhang et al. extended the model by introducing point-to-edge distances, leading to the development of the LOAM framework [15]. Variants such as LeGO-LOAM [16] and F-LOAM [17] were further optimized for structured and unstructured environments, respectively. In parallel, surfel-based SLAM systems [18] have also emerged, with SuMa++ [19] enhancing them through the integration of fully convolutional neural networks for semantic information extraction. However, these methods can struggle in low-feature environments or when using LiDARs with a narrow field of view, prompting the need for more robust solutions.

To handle such challenges, a wave of more adaptive and computationally efficient LiDAR-inertial odometry (LIO)

methods has been proposed. FAST-LIO2 [1], built upon the iKD-tree [20], uses an iterative extended Kalman filter (iEKF) to perform real-time scan-to-map alignment, and later replaces handcrafted features with point-to-plane ICP over raw points, significantly improving generalization. Faster-LIO [3] introduced sparse incremental voxels (iVox) for faster updates and efficient nearest neighbor search. Kiss-ICP [4] relies on adaptive thresholding in a point-to-point ICP framework, combined with downsampling strategies to ensure both robustness and speed. To further tackle sensor-level challenges, Shi et al. [21] proposed a motion distortion elimination algorithm based on multioutput Gaussian process regression (MOGPR). iG-LIO [22] incorporated incremental G-ICP and voxel-based surface covariance estimation [23], maintaining accuracy while improving computational efficiency. IGE-LIO [24] expanded on this by integrating LiDAR intensity gradients, offering superior resilience in degenerate scenes. Other contributions such as Xu et al.'s intermittent VIO for degeneracy mitigation [25], LVINS's fusion of LiDAR and visual descriptors [26], and Doppler-based odometry with vehicle kinematics [27], further demonstrate the increasing depth and breadth of LIO research.

Recent methods continue to expand capabilities in dense mapping, fusion, and long-term deployment. SuIn-LIO [28] leverages invariant EKF and efficient surfel mapping to achieve high performance, while Tao et al. [29] proposed a point-to-likelihood HD map matching method to improve tunnel localization. Gao et al. [30] demonstrated robust fusion odometry using INS-centric multi-modal systems, and Wang et al. [31] developed a TSDF-based dense mapping pipeline with augmented LiDAR data. MM-LINS and BA-LINS [32] extend this progress through multi-map management and frame-to-frame bundle adjustment, respectively. SE-LIO [33] incorporates semantic cues and adaptive cylinder fitting for reliable navigation in forested areas, while TLS-SLAM [34] employs 3D Gaussian splatting to improve convergence in large-scale mapping. ININ-LIO [35] applies deep learning to reduce inertial drift, and methods like SGT-LLC [36] and UA-LIO [37] demonstrate advances in loop closure and uncertainty-aware odometry. Although these systems exhibit excellent localization accuracy and robustness, they remain limited to single-session operation [38]–[45], and do not yet address the broader challenges of life-long deployment and multi-session mapping in evolving environments [46]–[49].

B. Multi-Session

Recent research has increasingly focused on multi-session frameworks to overcome the limitations of single-session systems, addressing long-term mapping and localization challenges. These approaches enhance pose estimation by incorporating additional constraints and improve adaptability to dynamic environments. For instance, K. Koide et al. [11] developed a SLAM-based relocalization framework with an independent odometry module that leverages scan-to-map information to refine pose estimates. Similarly, Giseop Kim et al. [50] introduced a modular LiDAR-based life-long mapping framework tailored for urban environments. Their multi-session SLAM approach, which includes dynamic change

detection and change management, effectively manages trajectory errors while optimizing memory and computational costs by automatically segregating objects from large-scale point cloud maps.

Complementary methods further illustrate the benefits of multi-session strategies. Block-map-based localization [51] employs a factor graph that integrates IMU pre-integration and scan-matching factors to enhance localization accuracy, while a range-inertial localization algorithm [52] tightly couples scan-to-scan and scan-to-map registrations with IMU data within a sliding-window factor graph framework. LTA-OM [53] advances LiDAR SLAM with innovations such as complete loop detection and correction, false-positive loop closure rejection, long-term association mapping, and multisession localization—utilizing a corrected history map to achieve drift-free odometry at revisit locations. Additionally, LiLoc [54] presents a graph-based life-long localization framework that maintains a single central session and leverages multimodal factors for enhanced accuracy and timeliness. Building on these foundations, our proposed method supports life-long deployment by delivering online, accurate, and robust localization through prior maps, seamlessly integrating environmental changes and unmapped areas into the original map.

III. METHODOLOGY

This section covers key concepts, such as definitions for life-long map management, an improved data structure, the overall system framework, and the algorithmic implementation.

A. Definition

To establish a rigorous foundation, we first introduce the fundamental notations employed in this study. The state of the robot \mathbf{x} is denoted as:

$$\mathbf{x} = [\mathbf{R}^\top, \mathbf{p}^\top, \mathbf{v}^\top, \mathbf{b}^\top]^\top \quad (1)$$

where $\mathbf{R} \in SO(3)$ is the rotation matrix. $\mathbf{p} \in \mathbb{R}^3$ is the position vector. $\mathbf{v} \in \mathbb{R}^3$ is the speed vector. \mathbf{b} is the bias of IMU. The full robot pose is represented as $\mathbf{T} = (\mathbf{R}, \mathbf{p}) \in SE(3)$. Moreover, \mathbf{x} , $\hat{\mathbf{x}}$ and $\bar{\mathbf{x}}$ denote the ground-true, predicted and updated values of \mathbf{x} . B and M refer to the robot's body coordinate frame and the map coordinate frame.

Additionally, to effectively manage map updates and localization, we define the following map components. Let the map \mathcal{M} be generated from a set of poses \mathbf{T}_i and corresponding sensor data \mathbf{S}_i , where each scan $\mathbf{S}_i = \{\mathbf{p}_j \mid \mathbf{p}_j \in \mathbb{R}^3, j = 1, \dots, N_i\}$ is a point cloud of N_i 3D points.

(a) **Prior Map Points \mathcal{M}^p and Prior Blocks \mathcal{B}^p :**

$$\mathcal{M}^p = \bigcup_{i=1}^N \mathbf{T}_i \mathbf{S}_i, \quad \mathcal{B}^p = \mathcal{V}(\mathcal{M}^p),$$

where $\mathcal{V}(\mathcal{P})$ partitions a point set \mathcal{P} into its constituent voxel blocks. The prior map is the union of historical scans at their respective poses, and the voxel blocks containing \mathcal{M}^p form the prior blocks \mathcal{B}^p .

(b) **Temporary Map Points \mathcal{M}^t :**

$$\mathcal{M}^t = \mathbf{T}_k \mathbf{S}_k.$$

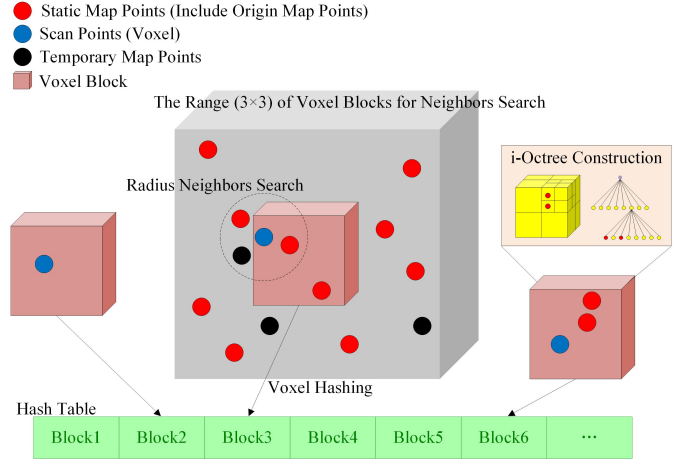


Fig. 2. Diagram of Dynamic i-Octree.

New scan points that do not match any in \mathcal{M}^s are added to \mathcal{M}^t , which serves as an auxiliary (backup) map for localization, complementing the static map. When the number of points in a voxel block exceeds a predefined threshold, these points are promoted to \mathcal{M}^s .

(c) **Static Map Points \mathcal{M}^s :**

$$\mathcal{M}^s = \mathcal{M}^p \cup \mathcal{M}^t.$$

During operation, points from \mathcal{M}^t may be promoted and points from \mathcal{M}^p removed according to an update policy. \mathcal{M}^s is the primary reference for localization and serves as the final output map.

B. Dynamic i-Octree

Efficiently managing these map points requires a robust structure. While Dynamic Octree [55] is effective for map management, it cannot determine when to update the map or which areas need updating, limiting its ability to switch between localization and map updates. To address this, we propose Dynamic i-Octree (see Fig. 2), a refined version of Dynamic Octree that efficiently handles randomly distributed points. By organizing the map based on the defined structure, Dynamic i-Octree enables dynamic local map loading, improving localization robustness and facilitating map updates. For better efficiency, we leverage i-Octree [56] to manage the points.

1) **Hash Pair (Key, Value):**

- Voxel (Key): \mathbf{p} of the point $p \in \mathbb{R}^3$ in M .
- Voxel Block (Value): the data contained in each voxel block includes \mathcal{M}^p , \mathcal{M}^t , \mathcal{M}^s and an i-Octree organized by \mathcal{M}^s for radius neighbor search.

2) **Hash Function Construction:** Define the voxel block index vector as:

$$\mathcal{B} = \begin{bmatrix} \mathcal{B}_x \\ \mathcal{B}_y \\ \mathcal{B}_z \end{bmatrix} = \begin{bmatrix} \lfloor \frac{p_x}{s} \rfloor \\ \lfloor \frac{p_y}{s} \rfloor \\ \lfloor \frac{p_z}{s} \rfloor \end{bmatrix} \quad (2)$$

where $p = [p_x, p_y, p_z]^\top \in \mathbb{R}^3$ is the 3D coordinate of the point in M . The parameter s is the resolution of each voxel

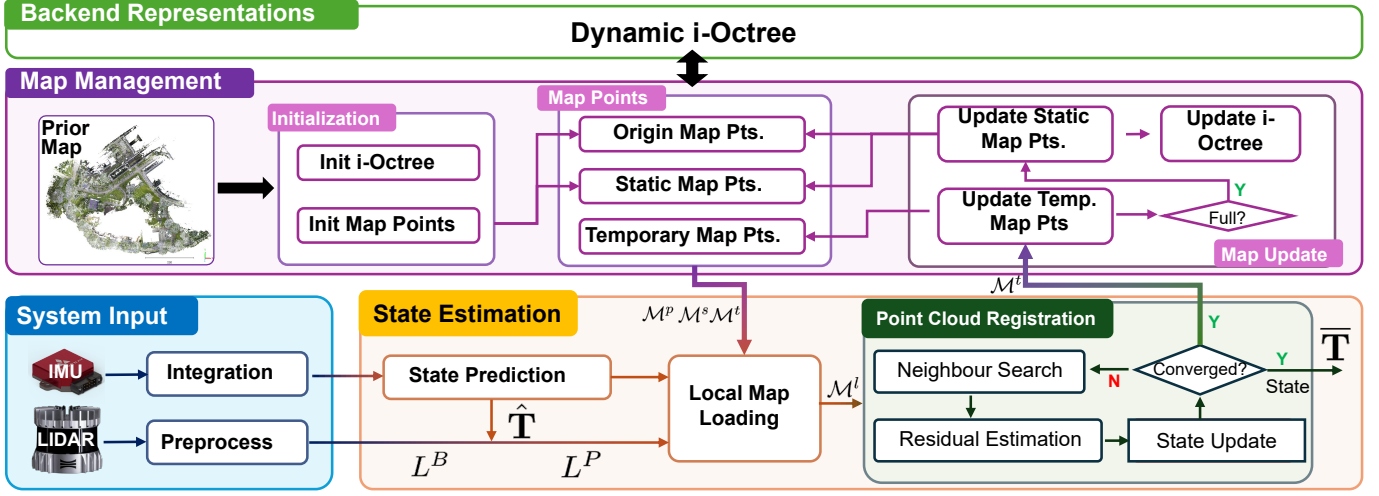


Fig. 3. System overview of LL-Localizer.

block. $\lfloor \cdot \rfloor$ denotes the floor function, which rounds down to the nearest integer. $\mathcal{B}_x, \mathcal{B}_y, \mathcal{B}_z$ are voxel block indices. The hash index for the voxel block is computed as:

$$\mathcal{H}_B = (\mathcal{B}_x \eta_x) \oplus (\mathcal{B}_y \eta_y) \oplus (\mathcal{B}_z \eta_z) \quad (3)$$

where \mathcal{H}_B represents the computed hash value. η_x, η_y and η_z are large prime numbers (e.g., $\eta_x = 73856093$, $\eta_y = 19349669$, $\eta_z = 83492791$) to reduce collisions and ensure good hashing properties. \oplus denotes the bitwise XOR operator.

3) *i-Octree*: In our system, we will retain the prior map as possible to ensure the accuracy of localization and map integrity, which will lead to significant differences in the density of points within the voxel blocks, with some voxel blocks having particularly high point densities. In this case, using *i-Octree* to organize \mathcal{M}^s for radius neighbor search instead of traversal can greatly improve the efficiency.

- (a) Implementation of *i-Octree*: we implement *i-Octree* in the voxel block, but we have made some modifications to *i-Octree* to make it more suitable for our system. Because we implement *i-Octree* in a voxel block of a certain size, the boundary of the axis-aligned bounding box of *i-Octree* is determined, we don't need to consider the situation that any points may be beyond the boundary. So we don't need to create new root octant to expand the bounding box. Besides, in order to preserve more of the prior map and maintain robustness in locating in areas without map, we have to sacrifice some efficiency to improve the accuracy of localization. Therefore, we only retained the downsampling function when inserting new points, but removed the Box-wise Delete function.
- (b) Radius Neighbor Search: for each query point $q \in \mathbb{R}^3$ and the radius of neighbor search r , radius neighbor search finds every point p satisfying $\|p - q\|_2 < r$. To accelerate radius neighbor search, *i-Octree* adopt the pruning strategy proposed by Behley et al. [57] with improvements to reduce computation cost. In addition, we further improve efficiency by parallel computing the radius neighbor search of each point in the scan.

C. System Framework

The overview of our proposed framework is shown in Fig. 3. Before running the robot, we load a prior map first. Then each point in this map will be added to \mathcal{M}^p and \mathcal{M}^s in the voxel block which it belongs to, and *i-Octree* will be constructed according to \mathcal{M}^s .

When the first few scans arrive, we merge them and then obtain the initial pose T_0 within the map using the global localization module Branch-and-Bound Search++ [51] (BBS++). During system operation, when a new LiDAR scan L^B arrives, the system transforms L^B according to the predicted pose \hat{T} to obtain L^P . It then dynamically loads the local map \mathcal{M}^l following the strategy (see Section III-E1), and performs point cloud registration to obtain accurate pose \bar{T} in M . After these processes, points in L^P that do not match \mathcal{M}^s will be added to the \mathcal{M}^t for future map updates. Once the size of \mathcal{M}^t in a voxel block reaches the predefined threshold, \mathcal{M}^s will be updated, and *i-Octree* will be updated accordingly (see Section III-E3). After the operation ends, \mathcal{M}^s will be output as the final result map.

D. IMU Integration

Through the high-frequency input of IMU data, the system can calculate the pose of the robot with more continuity.

The measurements of acceleration \hat{a} and angular velocity $\hat{\omega}$ from IMU at time t are defined as follows:

$$\hat{\alpha}_t = \alpha_t - g + \mathbf{b}_t^\alpha + n_t^\alpha \quad (4)$$

$$\hat{\omega}_t = \omega_t + \mathbf{b}_t^\omega + n_t^\omega \quad (5)$$

where $\hat{\alpha}_t$ and $\hat{\omega}_t$ denote the raw IMU measurements in B at t . The α_t and ω_t are the ground-truth values in B at t . g is the gravity vector in map frame M . The \mathbf{b} and n represent bias and white noise of IMU, respectively.

Then, the system can predict the state including the pose \mathbf{T}^P of the robot from time t to time $t + \Delta t$ until the next

LiDAR scan arrives as follows:

$$\hat{\mathbf{v}}_{t+\Delta t} = \hat{\mathbf{v}}_t + g\Delta t + \hat{\mathbf{R}}_t^{MB}(\hat{\alpha}_t - \mathbf{b}_t^\alpha - n_t^\alpha)\Delta t \quad (6)$$

$$\hat{\mathbf{p}}_{t+\Delta t} = \hat{\mathbf{p}}_t + \hat{\mathbf{v}}_t\Delta t + \frac{1}{2}g\Delta t^2 + \frac{1}{2}\hat{\mathbf{R}}_t^{MB}(\hat{\alpha}_t - \mathbf{b}_t^a - n_t^\alpha)\Delta t^2 \quad (7)$$

$$\hat{\mathbf{R}}_{t+\Delta t}^{MB} = \hat{\mathbf{R}}_t^{MB} \text{Exp}((\hat{\omega}_t - \mathbf{b}_t^\omega - n_t^\omega)\Delta t) \quad (8)$$

where $\text{Exp}(\omega) = \exp(\omega^\wedge)$, and $\exp(\cdot)$ is the exponential map function in $\text{SO}(3)$. $\hat{\mathbf{R}}_t^{MB}$ is the rotation matrix from baseframe B to map M at t . Based on the above calculation, the system can make a preliminary estimation of the robot's state.

E. Scan Process

Predicting the robot's pose solely based on IMU is not accurate enough, especially after long-duration and long-distance movements, where significant errors may accumulate. Therefore, we need to process LiDAR scans to correct the predicted pose \mathbf{T}^P . When a new scan arrives, system processes it through the following series of steps to achieve accurate localization and determine whether the map needs to be updated simultaneously.

1) *Local Map \mathcal{M}^l Loading Strategy*: With each incoming scan, the system loads the appropriate local map \mathcal{M}^l based on the scanned points. System first transform the point cloud from body coordinate to world coordinate through IMU integration. The system then locates the corresponding voxel block using the hash function in III-B2 and loads the appropriate map points from the three types of maps points to improve localization robustness. The loading strategy is mainly based on two criteria: the voxel block \mathcal{B}^r where the robot is located and the number *num* of scanned points in \mathcal{B}^p .

To evaluate the distribution of the scanned points, we first define the Heaviside Step function $H(x)$ as:

$$H(\mathcal{B}^r, \mathcal{B}^p) = \begin{cases} 0, & \mathcal{B}^r \in \mathcal{B}^p, \\ 1, & \mathcal{B}^r \notin \mathcal{B}^p. \end{cases} \quad (9)$$

Then, the effective distance ϕ^* can be defined as:

$$\phi^* = \phi_2 + (\phi_1 - \phi_2)H(\mathcal{B}^r, \mathcal{B}^p), \quad (10)$$

where ϕ_1 and ϕ_2 are predetermined factors, with $\phi_1 > \phi_2$. These factors can be adjusted to control the map loading strategy. They are initially chosen heuristically now and can be further optimized through a reinforcement learning framework to adapt to different environments and scanning conditions.

Next, we compute the ratio ρ to evaluate the spatial distribution of scanned points. For a LiDAR with a narrow field of view, we define ρ_n as:

$$\rho_n = \frac{\phi^{*2} \tan \frac{\theta_L}{2}}{\frac{1}{2} \times \phi_e \times \theta_L} \left(1 - 2H(\mathcal{B}^r, \mathcal{B}^p) \right) + H(\mathcal{B}^r, \mathcal{B}^p) \quad (11)$$

where:

- ϕ^* is the effective distance, as defined earlier.
- $\phi_e = d_{max}^2 - d_{min}^2$ is the effective range of the LiDAR.
- θ_L is the horizontal field of view of the LiDAR, (in Rad).

For a LiDAR with a 360° horizontal field of view, the ratio ρ_w is defined as:

$$\rho_w = \frac{1}{\pi d_{max}^2} \int_{-\sqrt{d_{max}^2 - \phi^{*2}}}^{\sqrt{d_{max}^2 - \phi^{*2}}} (\sqrt{d_{max}^2 - \mathbf{x}^2} - \phi^*) d\mathbf{x} \quad (12)$$

Finally, the threshold τ is computed as:

$$\tau = \lfloor n \times \rho \times s \rfloor \quad (13)$$

where:

- n is the number of scanned points.
- s is the resolution of each voxel block.
- ρ is the ratio selected from ρ_w or ρ_n based on the actual hardware.
- $\lfloor \cdot \rfloor$ denotes the floor function that rounds down to the nearest integer.

And we define a function $S(\cdot)$ to evaluate the convergence of point cloud registration:

$$S(r_k, k) = \begin{cases} 1, & r_k > \delta \ \& \ k \leq 10, \\ 0, & r_k > \delta \ \& \ k > 10. \end{cases} \quad (14)$$

where r_k denotes the residual at iteration k . δ is the predefined convergence threshold.

After computing the threshold τ and function $S(\cdot)$, the system determines the appropriate map loading strategy based on the voxel block \mathcal{B}^r where the robot is located, the number of scanned points κ in \mathcal{B}^p and point cloud registration convergence evaluation. Depending on these factors, the system can handle different localization scenarios as follows:

- (a) $\mathcal{B}^r \in \mathcal{B}^p$ and $\kappa \geq \tau$: We consider this to be the most ideal situation: the environment in prior map has not changed, or the subtle changes in the map can be ignored. In this case, system can only load \mathcal{M}^p in \mathcal{B}^p as the \mathcal{M}^l :

$$\mathcal{M}^l \subseteq \mathcal{M}^p$$

which can improve the efficiency of the system while achieving high robustness localization.

- (b) $\mathcal{B}^r \in \mathcal{B}^p$ and $\kappa < \tau$: We consider that the environment may have changed, or the robot may be moving out of the pre-mapped area into a non-mapped area. In this case, system will load \mathcal{M}^p in \mathcal{B}^p and \mathcal{M}^s in non \mathcal{B}^p as the \mathcal{M}^l :

$$\mathcal{M}^l \subseteq (\mathcal{M}^p \cup \mathcal{M}^s)$$

To ensure the robustness of localization, the system will trust the points in \mathcal{B}^p more, so we assign greater weight w^g to \mathcal{M}^p in \mathcal{B}^p in the residual calculation.

- (c) $\mathcal{B}^r \notin \mathcal{B}^p$ and $\kappa \geq \tau$: This occurs when the robot transitions from an unmapped area to a pre-mapped region. The system can directly load \mathcal{M}^p in \mathcal{B}^p as the \mathcal{M}^l to quickly eliminate positional drift accumulated during localization in unmapped area. However, if the drift error is too large, point cloud registration may fail to converge. In such cases, the system incorporates additional map data \mathcal{M}^s from outside \mathcal{B}^p to gradually eliminate the drift error:

$$\mathcal{M}^l \subseteq \begin{cases} \mathcal{M}^p, & S(r_k, k) = 1, \\ \mathcal{M}^p \cup \mathcal{M}^s, & S(r_k, k) = 0. \end{cases}$$

Similar to the previous case, we assign greater weight w^g to \mathcal{M}^p in \mathcal{B}^p during residual calculation.

- (d) $\mathcal{B}^r \notin \mathcal{B}^p$ and $\kappa < \tau$: This represents an extreme case where the robot may be navigating a new environment or the pre-mapped area has undergone significant changes. In this case, the system initially loads \mathcal{M}^s as the \mathcal{M}^l . If the information in \mathcal{M}^s is insufficient for point cloud registration to converge, the system incorporates additional map data \mathcal{M}^t into the \mathcal{M}^l :

$$\mathcal{M}^l \subseteq \begin{cases} \mathcal{M}^s, & S(r_k, k) = 1, \\ \mathcal{M}^s \cup \mathcal{M}^t, & S(r_k, k) = 0. \end{cases}$$

In the residual calculation, we assign a lower weight w^l to \mathcal{M}^t to reduce the impact of outliers.

Algorithm 1 Local Map Loading

Input: $\mathcal{M}^p, \mathcal{M}^s, \mathcal{M}^t$

Output: \mathcal{M}^l , weights for residual calculation w_n, w_g, w_l

```

1: Translate robot's  $\mathbf{T}$  from  $B$  to  $M$ 
2: if  $\mathcal{B}^r \in \mathcal{B}^p$  and  $\kappa \geq \tau$  then
3:    $\mathcal{M}^l \leftarrow \mathcal{M}^p \in \mathcal{B}^p$ 
4:    $\mathcal{M}^p \leftarrow w^n$ 
5: else if  $\mathcal{B}^r \in \mathcal{B}^p$  and  $\kappa < \tau$  then
6:    $\mathcal{M}^l \leftarrow \mathcal{M}^p \in \mathcal{B}^p, \mathcal{M}^l \leftarrow \mathcal{M}^s \notin \mathcal{B}^p$ 
7:    $\mathcal{M}^p \leftarrow w^g, \mathcal{M}^s \leftarrow w^n$ 
8: else if  $\mathcal{B}^r \notin \mathcal{B}^p$  and  $\kappa \geq \tau$  then
9:    $\mathcal{M}^l \leftarrow \mathcal{M}^p$  in  $\mathcal{B}^p$ 
10:   $\mathcal{M}^p \leftarrow w^n$ 
11:  if  $S(r_k, k) = 0$  then
12:     $\mathcal{M}^l \leftarrow \mathcal{M}^p \in \mathcal{B}^p, \mathcal{M}^l \leftarrow \mathcal{M}^s \notin \mathcal{B}^p$ 
13:     $\mathcal{M}^p \leftarrow w^g, \mathcal{M}^s \leftarrow w^n$ 
14:  end if
15: else if  $\mathcal{B}^r \notin \mathcal{B}^p$  and  $\kappa < \tau$  then
16:    $\mathcal{M}^l \leftarrow \mathcal{M}^s$ 
17:    $\mathcal{M}^s \leftarrow w^n$ 
18:   if  $S(r_k, k) = 0$  then
19:      $\mathcal{M}^l \leftarrow \mathcal{M}^s, \mathcal{M}^l \leftarrow \mathcal{M}^t$ 
20:      $\mathcal{M}^s \leftarrow w^n, \mathcal{M}^t \leftarrow w^l$ 
21:   end if
22: end if
```

2) *Point Matching and Point Cloud Registration:* After local map \mathcal{M}^l loading according to the strategy and radius neighbor search for the k -th scan, points $p_1, p_2, \dots, p_n \subseteq L_k^p$ obtain their corresponding neighbor points $Q_1, Q_2, \dots, Q_n \subseteq Q$. These neighbor points are then used to fit lines or planes. For a point $p^p \in (\mathcal{M}^l \cap Q)$ on the plane, its relationship with the plane parameters is given by:

$$\mathbf{n}^\top p^p + d = 0 \quad (15)$$

where \mathbf{n} is the normal vector of the plane with $|\mathbf{n}| = 1$, and the superscript $^\top$ denotes the transpose. d is the intercept. For a point $p^l \in (\mathcal{M}^l \cap Q)$ on the line, the equation of the line L can be expressed as:

$$L = \mathbf{d}x + p^l \quad (16)$$

where \mathbf{d} is the direction vector with $|\mathbf{d}| = 1$, and x is the scalar parameter used to determine the position of a point on

the line. Then we can formulate the error function between the i -th query point $p_i \in L_k^p$ and the fitted plane or line of its neighboring points:

$$r_i^p = w(\mathbf{n}^\top (\mathbf{R}p_i + \mathbf{p}) + d) \quad (17)$$

$$r_i^l = w(\mathbf{d} \times (\mathbf{R}p_i + \mathbf{p} - p^l)) \quad (18)$$

where r_i^p and r_i^l represent the residual from p_i to the fitted plane or line, respectively. w is the weight assigned according to III-E1 mentioned. Finally, the optimal \mathbf{R}^{MP} and \mathbf{p}^{MP} are obtained by iteratively minimizing the residual r until convergence:

$$r = \sum_n \|r_n^p\|^2 + \sum_m \|r_m^l\|^2 < \delta \quad (19)$$

when δ is the predefined convergence threshold.

3) *Map Update:* Unlike most LO/LIO systems, we do not directly update scanned points to the map. Due to the high accuracy of the prior map, we tend to trust prior maps more to prevent accumulated drift errors and reject outliers. We will only update the map when there are changes in the environment in prior map or when the robot is exploring an unknown environment.

If there are any points found no matching \mathcal{M}^s but the queried voxel blocks already exist, that means the voxel blocks which these points belong to may have changed. Or there is another situation that the robot scans an area outside the prior map so the queried voxel blocks do not exist. Both of these situations may have disastrous effects in current and future localization. Therefore, the map needs to be updated. But in our system, these points will be added to \mathcal{M}^t for temporary storage first. We do not directly add these points to the global map (i.e., \mathcal{M}^s) for the reason that they may be outliers, and we must reduce the effects of outliers in our system and trust the origin prior map more.

With the operation of the system, \mathcal{M}^t in each voxel block will accumulate incrementally. Once the size of \mathcal{M}^t in a voxel block reaches the predefined threshold, we assume that the environment in this voxel block changes or robot scans an area outside the prior map. Then system will add these \mathcal{M}^t to \mathcal{M}^s to update the map. After that, system will compare the size of \mathcal{M}^s and the size of \mathcal{M}^p in this updated voxel block if this voxel block is \mathcal{B}^p . If the size of \mathcal{M}^s is greater than twice the size of \mathcal{M}^p , also means that the size of \mathcal{M}^t is greater than the size of \mathcal{M}^p , we assert the environment in this voxel block in prior map undergoes drastic changes and the prior map is unreliable. Then system will clear the \mathcal{M}^s in this voxel block and add \mathcal{M}^t to \mathcal{M}^s again, and then set this \mathcal{B}^p as a non \mathcal{B}^p . After updating the voxel block, the system will clear the \mathcal{M}^t and update i-Octree according to new \mathcal{M}^s .

IV. EXPERIMENTS

A. Datasets, Prior Map Reconstructions, and Baselines

Datasets: The proposed system is evaluated using three widely used datasets: the North Campus Long-Term dataset (NCLT) [58], M2DGR [59], and the Botanic Garden dataset (BG) [60]. Each dataset contains multiple sequences recorded

at the same location under varying environmental conditions, including different scene setups, dynamic objects, and structural changes. Table I summarizes the recording dates, environments, and trajectory distances for each dataset. We use the EVO [61] trajectory evaluation tool to verify the system’s precision and robustness.

TABLE I
SEQUENCES AND ENVIRONMENTS

Seq.	Date	Environment	Dist.(kilometer)
nclt_1	2012.4.29	long-term, dynamic objects	3.186
nclt_2	2012.6.15	long-term, dynamic objects	4.106
nclt_3	2013.1.10	long-term, dynamic objects	1.139
nclt_4	2012.5.11	long-term, dynamic objects	6.120
gate_1	2021.8.4	open square, dynamic objects	0.248
gate_2	2021.7.31	open square, dynamic objects	0.139
gate_3	2021.7.31	open square, dynamic objects	0.289
street_1	2021.8.6	open square, dynamic objects	0.340
street_2	2021.8.6	open square, dynamic objects	0.752
street_3	2021.8.6	open square, dynamic objects	0.423
bg_1	2022.10.8	unstructured tree, platform vibrations	0.855
bg_2	2022.10.5	unstructured tree, platform vibrations	0.566
bg_3	2022.10.6	unstructured tree, platform vibrations	0.686

Prior Map Reconstructions: To assess the system’s ability to handle long-term environmental changes, we construct the prior map using the first sequence (**sequence_1**) from each dataset. The remaining sequences simulate life-long deployment scenarios, where the system is tested under evolving environmental conditions. This setup allows us to evaluate how well the system adapts to changing environments and maintains accurate localization.

Comparison Selections: We surveyed the literature for existing LIO methods. Many prior works either do not provide open-source implementations [21], [28]–[30], [32]–[35], [38], [47], [62], [63], or their codebases are no longer maintained and cannot be successfully built [27], [31], [37]. Other methods [64]–[68] are less relevant to our setting, as they require additional sensory inputs or networks that are not directly compatible with our system [24]–[26], [36], [42], [44], [46], [48], [69]–[72]. Ultimately, we selected Fast-LIO2 [1], Fast-LIO-SLAM (Fast-LIO2 with Scan Context based loop closure [73]), Faster-LIO [3], F-LOAM [74] and iG-LIO [22] as our baseline, given their open-source implementation and support for loop closure or incremental registration, which makes them well-suited for large-scale environments. Additionally, we compare our system against four map-based localization systems, including HDL-Loc [11], Fast-LIO-Loc (map-based localization method extended from Fast-LIO2), LT-AOM [53], and LiLoc [54]. Among these, the map-based localization systems and our proposed system perform localization using a prior map, whereas the SLAM systems perform simultaneous localization and mapping(with loop closure).

B. Life-long Deployment

We evaluate the robustness of our proposed system in life-long deployment by examining its performance under environmental variations.

As illustrated in Fig. 1, the environment represented by the prior map naturally evolves due to factors such as parked vehicles and growing trees. Our system is capable of dynamically updating the map to reflect these changes and can also extend the map to previously unmapped areas. Importantly, our map update strategy is designed to minimize the inclusion of dynamic objects, such as passing vehicles and pedestrians, which helps reduce their negative impact on both mapping and localization accuracy.

Table II presents the Absolute Pose Error (APE) results for each system. We evaluate the error using root-mean-square error (RMSE) and maximum error, calculated from the trajectory results of each system against the ground-truth using the EVO package [61]. As shown in Table II, with the guidance of prior knowledge, map-based localization methods demonstrate higher localization accuracy compared to SLAM systems that operate without prior map. However, map-based localization methods still have limitations. For example, HDL-Loc fails when the system encounters areas without prior map due to its inability to update maps. LiLoc, although capable of updating maps, struggles in dynamic environments such as parking lots with rapidly changing conditions, owing to the delay in map updates. In contrast, our system effectively handles both scenarios by dynamically loading local maps and applying the three-layer map management approach. Additionally, even in the presence of dynamic objects and significant platform vibrations, which could mislead localization and degrade performance, our system remains minimally affected and maintains robust localization due to its adaptive map updating strategy.

And as Fig. 4 and Fig. 5 show, our system effectively mitigates the impact of platform vibrations on motion estimation and maintains robust and high-precision localization even in a botanical garden with numerous unstructured trees.

C. Exploring Unknown Environments / Incomplete Map

This section further verifies the accuracy and robustness of the proposed system in various environments.

To simulate the scenario that the robot traverses from the pre-mapped area to the non-mapped area, stays there for a long period, and then returns to the pre-mapped area, we cropped most of the map of nclt_4 and conducted the experiment within this modified map. During the operation in the non-mapped area, factors such as random pedestrians, dynamic vehicles, and unstructured trees affect the accuracy of localization. Facing these challenges, the trajectory of the robot may accumulate drift after a long period of movement.

In this experiment, Hdl-Loc [11] still fails after entering an area without prior map due to its inability to switch from map-based localization mode to SLAM mode. Fast-LIO-Loc, LTAOM [53] and LiLoc [54] can switch to SLAM mode for map updates; however, their update strategy simply adds scanned point cloud to the map. As a result, even with downsampling process, they still retain many ghost point clouds caused by dynamic objects in the map. As for the SLAM systems Fast-LIO2 [1] and Fast-LIO-SLAM, their localization accuracy in mapped areas is inferior to map-based localization methods

TABLE II
ABSOLUTE POSE ERROR IN TERMS OF RMSE AND MAX ERROR (METER). THE BEST RESULTS ARE IN **BOLD**.

Seq.	nclt_2		nclt_3		gate_2		gate_3		street_2		street_3		bg_2		bg_3	
	RMSE	Max	RMSE	Max	RMSE	Max	RMSE	Max	RMSE	Max	RMSE	Max	RMSE	Max	RMSE	Max
F-LOAM [74]	×	×	×	×	×	×	×	×	×	×	×	×	×	×	×	×
Hdl-Loc [11]	×	×	×	×	0.168	1.159	0.328	1.028	×	×	0.176	0.423	×	×	×	×
Fast-LIO-Loc	1.988	3.990	0.911	2.060	0.153	0.359	0.313	0.965	0.299	0.688	0.183	0.449	0.523	1.477	0.358	0.896
LTA-OM [53]	2.185	6.156	1.648	5.290	0.222	0.598	0.414	0.977	0.328	0.722	0.183	0.465	0.467	1.051	0.636	1.507
LiLoc [54]	×	×	×	×	0.138	0.315	0.366	1.005	0.480	0.964	0.129	0.261	0.465	1.164	0.585	1.474
Fast-LIO2 [1]	2.006	3.887	0.912	2.061	0.154	0.349	0.322	0.975	0.299	0.676	0.149	0.503	0.672	1.491	0.350	0.847
Fast-LIO-SLAM	×	×	×	×	0.545	0.944	0.341	0.952	5.102	9.263	0.205	0.578	0.844	2.298	0.729	3.375
Faster-LIO [3]	1.614	3.477	0.941	2.291	1.337	1.716	1.268	1.976	0.825	1.631	1.175	1.703	1.331	1.829	1.047	1.442
iG-LIO [22]	1.565	4.032	1.148	2.619	0.117	0.291	0.322	0.996	0.287	0.664	0.126	0.238	×	×	×	×
LL-Localizer (Ours)	1.529	3.989	0.888	2.303	0.164	0.395	0.312	0.807	0.283	0.633	0.152	0.526	0.255	0.642	0.239	0.554

¹ “×” indicates system failure due to unrecoverable drift ($\geq 10\%$ distance error) or numerical instability.

² Fast-LIO-Loc is a map-based localization method adapted from Fast-LIO2 in our deployment.

³ Fast-LIO-SLAM is our own implementation of Fast-LIO2 with Scan Context.

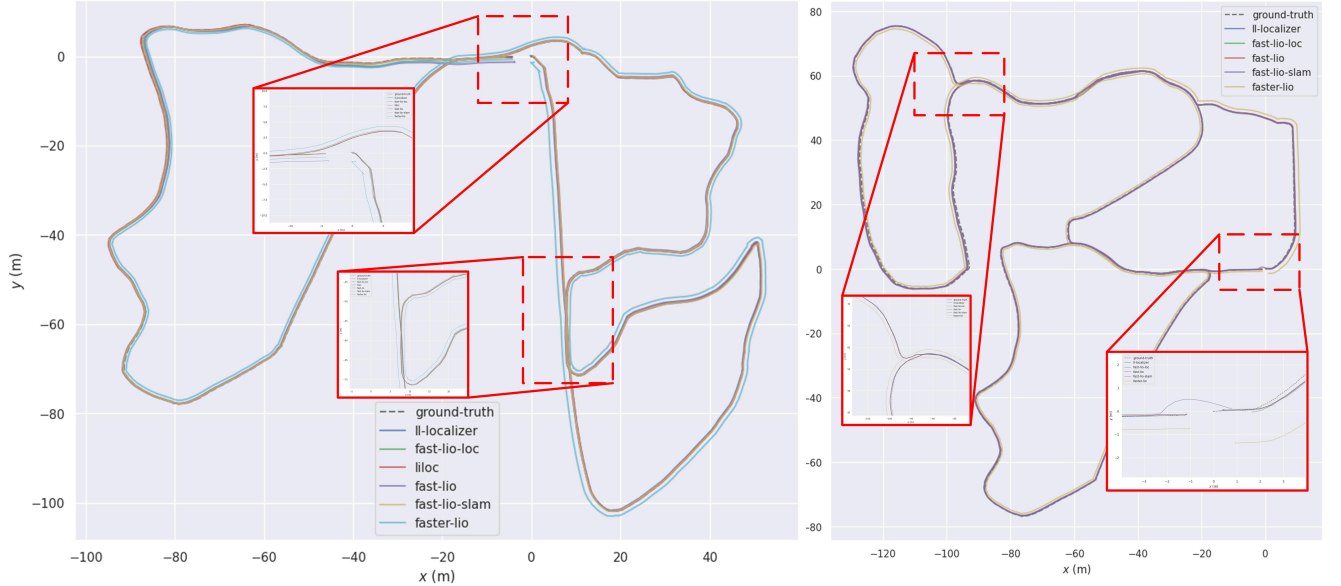


Fig. 4. The trajectory results of different systems in bg_2 (left) and bg_3 (right).

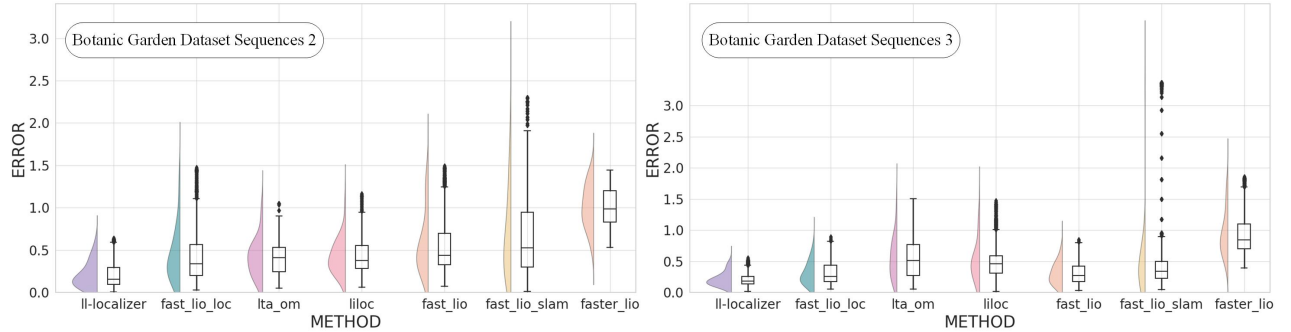


Fig. 5. The error of different systems in bg_2 (left) and bg_3 (right).

due to the lack of prior knowledge. In particular, Fast-LIO-SLAM’s Scan Context-based loop closure occasionally fails, leading to severe localization errors. But from Fig. 6, it can be seen that LL-Localizer maintains consistently high and excellent localization accuracy in both pre-mapped and non-mapped areas, and achieves updating consistent map after a long period of movement.

D. Time Cost Evaluation

We conduct experiments using three different methods: managing points within each voxel block using i-Octree, using static Octree, and not using any data structure for point management. After finding the corresponding voxel block via hash function, these three methods perform radius neighbor search using i-Octree, static Octree and traversal, respectively.

As Table III shows, compared to traversal and static Oc-

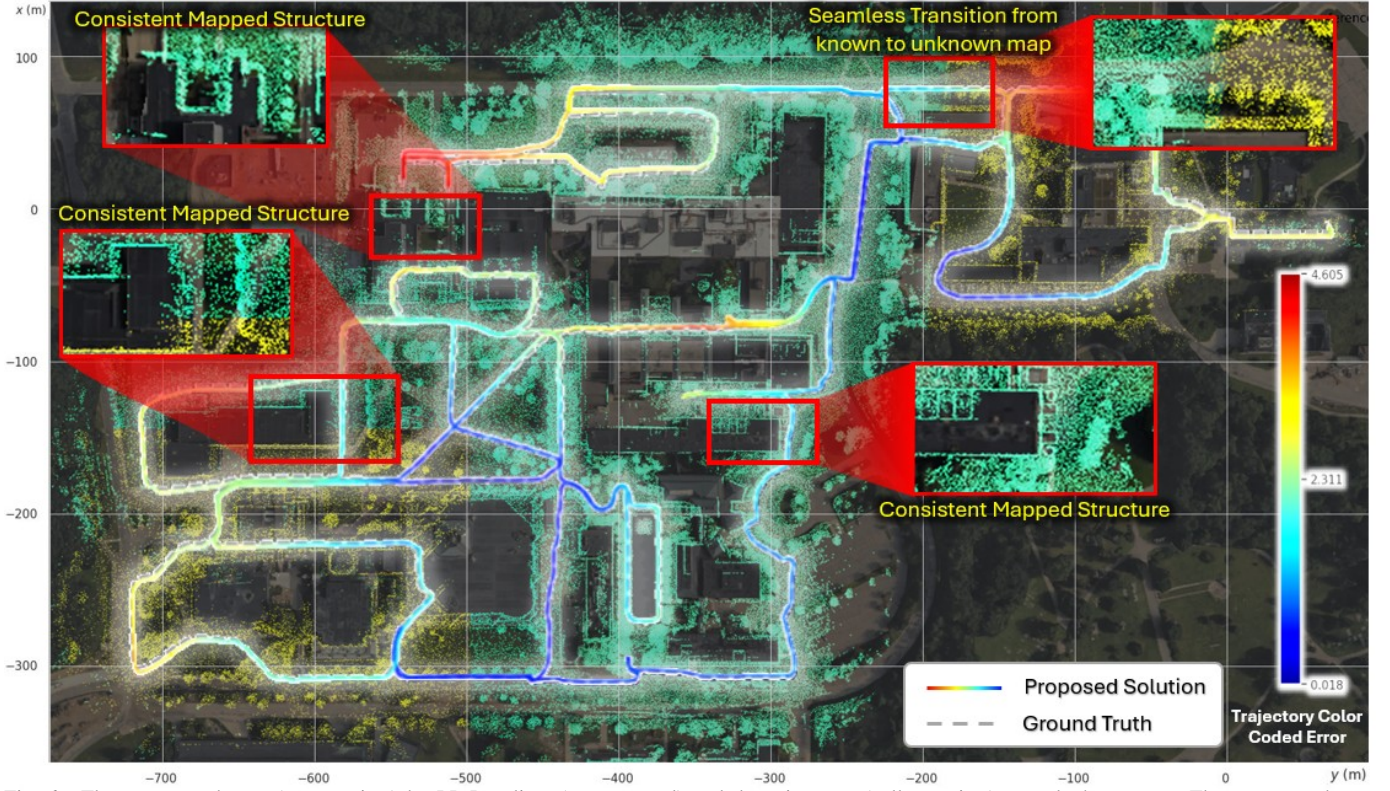


Fig. 6. The constructed map (green points) by LL-Localizer (our proposal) and the prior map (yellow points) on nclt_4 sequence. The constructed map is compared with the corresponding satellite image. The colorful line shows the trajectory and errors of our proposal, and the dashed line represents the ground-truth trajectory.

tree, i-Octree improves the efficiency of system processing, including neighbor searches and updates of voxel blocks. In radius neighbor search, i-Octree and static Octree exhibit similar efficiency, both significantly outperforming traversal. Additionally, due to its incremental update mechanism, i-Octree achieves faster update efficiency compared to Static Octree. By using Dynamic i-Octree, the majority of frames can be processed within 80ms, and even in dense maps, the system can still maintain real-time operation.

TABLE III
TIME COST (MILLISECOND) AND PROPORTION OF TIME > 80MS (%)
COMPARISON

Seq.	i-Octree		traverse		static Octree	
	Mean	>80ms	Mean	>80ms	Mean	>80ms
nclt_2	58.37	18.96	88.61	56.45	76.02	40.07
nclt_3	56.38	15.21	78.48	43.60	74.50	38.71
nclt_4	51.53	10.14	70.01	30.56	67.76	27.34
gate_2	62.73	21.00	95.30	70.65	85.20	67.31
gate_3	63.64	27.91	79.57	47.60	73.53	43.59
street_2	64.23	20.28	92.96	66.79	80.24	64.27
street_3	68.73	27.85	91.91	67.54	84.51	64.85
bg_2	48.83	7.88	70.25	31.61	62.49	20.91
bg_3	38.16	1.61	56.59	11.63	54.42	9.79

V. CONCLUSION

This letter presents LL-Localizer, a method for life-long localization utilizing prior maps based on incremental voxel.

The framework we proposed allows robots to maintain robust and accurate localization even when the environment changes or they traverses between mapped and unmapped areas, without the ability of environmental perception. And it can simultaneously update the maps of areas where the environment has changed and areas without maps. In addition, we utilised Dynamic i-Octree, which is an improvement from Dynamic Octree. This data structure is very suitable for our map management method and can maintain accurate and efficient neighbor search in maps of different densities through hash map and i-Octree even in dense maps. Contrast experiments in public datasets verifies that LL-Localizer can perform stable and accurate localization comparable to state-of-the-art localization systems in different environments. And even if the environment in the prior map changes or the robots traverses between mapped and unmapped areas, our system can still maintain consistently robust and accurate localization.

REFERENCES

- [1] W. Xu, Y. Cai, D. He, J. Lin, and F. Zhang, "Fast-lio2: Fast direct lidar-inertial odometry," *IEEE Transactions on Robotics*, vol. 38, no. 4, pp. 2053–2073, 2022.
- [2] K. Chen, R. Nemiroff, and B. T. Lopez, "Direct lidar-inertial odometry: Lightweight lio with continuous-time motion correction," in *2023 IEEE international conference on robotics and automation (ICRA)*. IEEE, 2023, pp. 3983–3989.
- [3] C. Bai, T. Xiao, Y. Chen, H. Wang, F. Zhang, and X. Gao, "Faster-lio: Lightweight tightly coupled lidar-inertial odometry using parallel sparse incremental voxels," *IEEE Robotics and Automation Letters*, vol. 7, no. 2, pp. 4861–4868, 2022.
- [4] I. Vizzo, T. Guadagnino, B. Mersch, L. Wiesmann, J. Behley, and C. Stachniss, "Kiss-icp: In defense of point-to-point icp – simple,

- accurate, and robust registration if done the right way,” *IEEE Robotics and Automation Letters*, vol. 8, no. 2, pp. 1029–1036, 2023.
- [5] Y. Zhang, Y. Tian, W. Wang, G. Yang, Z. Li, F. Jing, and M. Tan, “Ri-lio: Reflectivity image assisted tightly-coupled lidar-inertial odometry,” *IEEE Robotics and Automation Letters*, vol. 8, no. 3, pp. 1802–1809, 2023.
 - [6] X. Zheng and J. Zhu, “Traj-lio: In defense of lidar-only odometry using an effective continuous-time trajectory,” *IEEE Robotics and Automation Letters*, vol. 9, no. 2, pp. 1961–1968, 2024.
 - [7] Z. Yuan, F. Lang, T. Xu, R. Ming, C. Zhao, and X. Yang, “Semi-elastic lidar-inertial odometry,” in *Proceedings of the IEEE International Conference on Robotics and Automation (ICRA)*. IEEE, 2025.
 - [8] X. Zheng and J. Zhu, “Traj-lio: A resilient multi-lidar multi-imu state estimator through sparse gaussian process,” *arXiv preprint arXiv:2402.09189*, 2024.
 - [9] A. Tao, Y. Luo, C. Xia, C. Guo, and X. Li, “Equivariant filter for tightly coupled lidar-inertial odometry,” in *Proceedings of the IEEE International Conference on Robotics and Automation (ICRA)*. IEEE, 2025.
 - [10] P. Egger, P. V. K. Borges, G. Catt, A. Pfrunder, R. Siegwart, and R. Dubé, “Posemap: Lifelong, multi-environment 3d lidar localization,” in *2018 IEEE/RSJ International Conference on Intelligent Robots and Systems (IROS)*, 2018, pp. 3430–3437.
 - [11] K. Koide, J. Miura, and E. Menegatti, “A portable three-dimensional lidar-based system for long-term and wide-area people behavior measurement,” *International Journal of Advanced Robotic Systems*, vol. 16, no. 2, p. 1729881419841532, 2019.
 - [12] P. J. Besl and N. D. McKay, “Method for registration of 3-D shapes,” in *Sensor Fusion IV: Control Paradigms and Data Structures*, P. S. Schenker, Ed., vol. 1611, International Society for Optics and Photonics. SPIE, 1992, pp. 586 – 606. [Online]. Available: <https://doi.org/10.1117/12.57955>
 - [13] G. Sharp, S. Lee, and D. Wehe, “Icp registration using invariant features,” *IEEE Transactions on Pattern Analysis and Machine Intelligence*, vol. 24, no. 1, pp. 90–102, 2002.
 - [14] A. Segal, D. Haehnel, and S. Thrun, “Generalized-icp,” in *Robotics: science and systems*, vol. 2, no. 4. Seattle, WA, 2009, p. 435.
 - [15] J. Zhang, S. Singh *et al.*, “Loam: Lidar odometry and mapping in real-time,” in *Robotics: Science and systems*, vol. 2, no. 9. Berkeley, CA, 2014, pp. 1–9.
 - [16] T. Shan and B. Englot, “Lego-loam: Lightweight and ground-optimized lidar odometry and mapping on variable terrain,” in *2018 IEEE/RSJ International Conference on Intelligent Robots and Systems (IROS)*. IEEE, 2018, pp. 4758–4765.
 - [17] H. Wang, C. Wang, C.-L. Chen, and L. Xie, “F-loam: Fast lidar odometry and mapping,” in *2021 IEEE/RSJ International Conference on Intelligent Robots and Systems (IROS)*. IEEE, 2021, pp. 4390–4396.
 - [18] J. Behley and C. Stachniss, “Efficient surfel-based slam using 3d laser range data in urban environments,” in *Robotics: science and systems*, vol. 2018, 2018, p. 59.
 - [19] X. Chen, A. Milioto, E. Palazzolo, P. Giguere, J. Behley, and C. Stachniss, “Suma++: Efficient lidar-based semantic slam,” in *2019 IEEE/RSJ International Conference on Intelligent Robots and Systems (IROS)*. IEEE, 2019, pp. 4530–4537.
 - [20] Y. Cai, W. Xu, and F. Zhang, “ikd-tree: An incremental kd tree for robotic applications,” *arXiv preprint arXiv:2102.10808*, 2021.
 - [21] J. Shi, W. Wang, X. Li, Y. Yan, and E. Yin, “Motion distortion elimination for lidar-inertial odometry under rapid motion conditions,” *IEEE Transactions on Instrumentation and Measurement*, vol. 72, pp. 1–16, 2023.
 - [22] Z. Chen, Y. Xu, S. Yuan, and L. Xie, “ig-lio: An incremental gicp-based tightly-coupled lidar-inertial odometry,” *IEEE Robotics and Automation Letters*, vol. 9, no. 2, pp. 1883–1890, 2024.
 - [23] C. Yuan, W. Xu, X. Liu, X. Hong, and F. Zhang, “Efficient and probabilistic adaptive voxel mapping for accurate online lidar odometry,” *IEEE Robotics and Automation Letters*, vol. 7, no. 3, pp. 8518–8525, 2022.
 - [24] Z. Chen, H. Zhu, B. Yu, C. Jiang, C. Hua, X. Fu, and X. Kuang, “Ige-lio: Intensity gradient enhanced tightly-coupled lidar-inertial odometry,” *IEEE Transactions on Instrumentation and Measurement*, 2024.
 - [25] J. Xu, T. Li, H. Wang, Z. Wang, T. Bai, and X. Hou, “Intermittent vio-assisted lidar slam against degeneracy: Recognition and mitigation,” *IEEE Transactions on Instrumentation and Measurement*, 2024.
 - [26] X. Zhao, C. Wen, S. M. Prakhya, H. Yin, R. Zhou, Y. Sun, J. Xu, H. Bai, and Y. Wang, “Multi-modal features and accurate place recognition with robust optimization for lidar-visual-inertial slam,” *IEEE Transactions on Instrumentation and Measurement*, 2024.
 - [27] C. Pang, Z. Shen, R. Wu, and Z. Fang, “Efficient doppler lidar odometry using scan slicing and vehicle kinematics,” *IEEE Transactions on Instrumentation and Measurement*, 2024.
 - [28] H. Zhang, R. Xiao, J. Li, C. Yan, and H. Tang, “A high-precision lidar-inertial odometry via invariant extended kalman filtering and efficient surfel mapping,” *IEEE Transactions on Instrumentation and Measurement*, 2024.
 - [29] Q. Tao, Z. Hu, Y. Liu, and Z. Zhu, “Lidar-based localization in tunnel from hd map matching with pavement marking likelihood,” *IEEE Transactions on Instrumentation and Measurement*, 2024.
 - [30] J. Gao, J. Sha, H. Li, and Y. Wang, “A robust and fast gnss-inertial-lidar odometry with ins-centric multiple modalities by ieskf,” *IEEE Transactions on Instrumentation and Measurement*, vol. 73, pp. 1–12, 2024.
 - [31] J. Wang, M. Xu, and Z. Chen, “Range map interpolation based 3d lidar truncated signed distance fields mapping in outdoor environments,” *IEEE Transactions on Instrumentation and Measurement*, 2024.
 - [32] H. Tang, T. Zhang, L. Wang, M. Yuan, and X. Niu, “Ba-lins: A frame-to-frame bundle adjustment for lidar-inertial navigation,” *IEEE Transactions on Intelligent Transportation Systems*, 2025.
 - [33] T. Zhang, L. Wei, H. Tang, M. Yuan, L. Wang, and X. Niu, “Se-lio: Semantic-enhanced solid-state-lidar-inertial odometry for tree-rich environments,” *IEEE Transactions on Instrumentation and Measurement*, 2025.
 - [34] S. Cheng, S. He, F. Duan, and N. An, “Tls-slam: Gaussian splatting slam tailored for large-scale scenes,” *IEEE Robotics and Automation Letters*, 2025.
 - [35] Y. Gao, L. Zhao, and B. Zhang, “Inin-lio: Informer-based neural inertial network aided lidar-inertial odometry,” *IEEE Transactions on Instrumentation and Measurement*, 2025.
 - [36] S. Wang, F. Cao, T. Wang, X. Chen, and S. Shao, “Sgt-llc: Lidar loop closing based on semantic graph with triangular spatial topology,” *IEEE Robotics and Automation Letters*, 2025.
 - [37] Q. Wu, X. Chen, X. Xu, X. Zhong, X. Qu, S. Xia, G. Liu, L. Liu, W. Yu, and L. Pei, “Ua-lio: An uncertainty-aware lidar-inertial odometry for autonomous driving in urban environments,” *IEEE Transactions on Instrumentation and Measurement*, 2025.
 - [38] T.-M. Nguyen, M. Cao, S. Yuan, Y. Lyu, T. H. Nguyen, and L. Xie, “Viral-fusion: A visual-inertial-ranging-lidar sensor fusion approach,” *IEEE Transactions on Robotics*, vol. 38, no. 2, pp. 958–977, 2021.
 - [39] B. Lou, S. Yuan, J. Yang, W. Su, Y. Zhang, and E. Hu, “Qlio: Quantized lidar-inertial odometry,” *arXiv preprint arXiv:2503.07949*, 2025.
 - [40] X. Ji, S. Yuan, J. Li, P. Yin, H. Cao, and L. Xie, “Sgba: Semantic gaussian mixture model-based lidar bundle adjustment,” *IEEE Robotics and Automation Letters*, 2024.
 - [41] Y. Tao, Y. Bhalgat, L. F. T. Fu, M. Mattamala, N. Chebrolu, and M. Fallon, “Silvr: Scalable lidar-visual reconstruction with neural radiance fields for robotic inspection,” in *2024 IEEE International Conference on Robotics and Automation (ICRA)*. IEEE, 2024, pp. 17983–17989.
 - [42] C. Zhao, K. Hu, J. Xu, L. Zhao, B. Han, K. Wu, M. Tian, and S. Yuan, “Adaptive-lio: Enhancing robustness and precision through environmental adaptation in lidar inertial odometry,” *IEEE Internet of Things Journal*, 2024.
 - [43] W. Yu, J. Xu, C. Zhao, L. Zhao, T.-M. Nguyen, S. Yuan, M. Bai, and L. Xie, “I 2 ekf-lo: A dual-iteration extended kalman filter based lidar odometry,” in *2024 IEEE/RSJ International Conference on Intelligent Robots and Systems (IROS)*. IEEE, 2024, pp. 10453–10460.
 - [44] J. Xu, W. Yu, S. Huang, S. Yuan, L. Zhao, R. Li, and L. Xie, “M-divo: Multiple tof rgb-d cameras-enhanced depth-inertial-visual odometry,” *IEEE Internet of Things Journal*, vol. 11, no. 23, pp. 37562–37570, 2024.
 - [45] H. Cai, S. Yuan, X. Li, J. Guo, and J. Liu, “Bev-lio (lc): Bev image assisted lidar-inertial odometry with loop closure,” *arXiv preprint arXiv:2502.19242*, 2025.
 - [46] F. Zhu, Y. Ren, L. Yin, F. Kong, Q. Liu, R. Xue, W. Liu, Y. Cai, G. Lu, H. Li *et al.*, “Swarm-lid2: Decentralized, efficient lidar-inertial odometry for uav swarms,” *IEEE Transactions on Robotics*, 2024.
 - [47] R. Border, N. Chebrolu, Y. Tao, J. D. Gammell, and M. Fallon, “Osprey: Multi-session autonomous aerial mapping with lidar-based slam and next best view planning,” *IEEE Transactions on Field Robotics*, 2024.
 - [48] L. Li, S. Peng, Z. Yu, S. Liu, R. Pautrat, X. Yin, and M. Pollefeys, “3d neural edge reconstruction,” in *Proceedings of the IEEE/CVF Conference on Computer Vision and Pattern Recognition*, 2024, pp. 21219–21229.
 - [49] J. Li, Q. Leng, J. Liu, X. Xu, T. Jin, M. Cao, T.-M. Nguyen, S. Yuan, K. Cao, and L. Xie, “Helmetposer: A helmet-mounted imu dataset for data-driven estimation of human head motion in diverse conditions,” in

- Proceedings of the 2025 IEEE International Conference on Robotics and Automation (ICRA)*, Atlanta, USA, May 2025.
- [50] G. Kim and A. Kim, "Lt-mapper: A modular framework for lidar-based lifelong mapping," in *2022 International Conference on Robotics and Automation (ICRA)*. IEEE, 2022, pp. 7995–8002.
 - [51] Y. Feng, Z. Jiang, Y. Shi, Y. Feng, X. Chen, H. Zhao, and G. Zhou, "Block-map-based localization in large-scale environment," in *2024 IEEE International Conference on Robotics and Automation (ICRA)*. IEEE, 2024, pp. 1709–1715.
 - [52] K. Koide, S. Oishi, M. Yokozuka, and A. Banno, "Tightly coupled range inertial localization on a 3d prior map based on sliding window factor graph optimization," in *2024 IEEE International Conference on Robotics and Automation (ICRA)*. IEEE, 2024, pp. 1745–1751.
 - [53] Z. Zou, C. Yuan, W. Xu, H. Li, S. Zhou, K. Xue, and F. Zhang, "Lta-om: Long-term association lidar-imu odometry and mapping," *Journal of Field Robotics*, vol. 41, no. 7, pp. 2455–2474, 2024.
 - [54] Y. Fang, Y. Li, K. Qian, F. Tombari, Y. Wang, and G. H. Lee, "Liloc: Lifelong localization using adaptive submap joining and egocentric factor graph," *arXiv preprint arXiv:2409.10172*, 2024.
 - [55] S. Zhao, H. Zhang, P. Wang, L. Nogueira, and S. Scherer, "Super odometry: Imu-centric lidar-visual-inertial estimator for challenging environments," in *2021 IEEE/RSJ International Conference on Intelligent Robots and Systems (IROS)*. IEEE, 2021, pp. 8729–8736.
 - [56] J. Zhu, H. Li, Z. Wang, S. Wang, and T. Zhang, "i-octree: A fast, lightweight, and dynamic octree for proximity search," in *2024 IEEE International Conference on Robotics and Automation (ICRA)*. IEEE, 2024, pp. 12 290–12 296.
 - [57] J. Behley, V. Steinhage, and A. B. Cremers, "Efficient radius neighbor search in three-dimensional point clouds," in *2015 IEEE international conference on robotics and automation (ICRA)*. IEEE, 2015, pp. 3625–3630.
 - [58] N. Carlevaris-Bianco, A. K. Ushani, and R. M. Eustice, "University of michigan north campus long-term vision and lidar dataset," *The International Journal of Robotics Research*, vol. 35, no. 9, pp. 1023–1035, 2016.
 - [59] J. Yin, A. Li, T. Li, W. Yu, and D. Zou, "M2dgr: A multi-sensor and multi-scenario slam dataset for ground robots," *IEEE Robotics and Automation Letters*, vol. 7, no. 2, pp. 2266–2273, 2021.
 - [60] Y. Liu, Y. Fu, M. Qin, Y. Xu, B. Xu, F. Chen, B. Goossens, H. Yu, C. Liu, L. Chen *et al.*, "Botanicgarden: A high-quality and large-scale robot navigation dataset in challenging natural environments," *arXiv preprint arXiv:2306.14137*, 2023.
 - [61] M. Grupp, "Evo: Python package for the evaluation of odometry and slam," <https://github.com/MichaelGrupp/evo>, 2017.
 - [62] J. Li, T.-M. Nguyen, S. Yuan, and L. Xie, "Pss-ba: Lidar bundle adjustment with progressive spatial smoothing," in *2024 IEEE/RSJ International Conference on Intelligent Robots and Systems (IROS)*. IEEE, 2024, pp. 1124–1129.
 - [63] J. Li, S. Yuan, M. Cao, T.-M. Nguyen, K. Cao, and L. Xie, "Hcto: Optimality-aware lidar inertial odometry with hybrid continuous time optimization for compact wearable mapping system," *ISPRS Journal of Photogrammetry and Remote Sensing*, vol. 211, pp. 228–243, 2024.
 - [64] K. Xu, Y. Hao, S. Yuan, C. Wang, and L. Xie, "Airlslam: An efficient and illumination-robust point-line visual slam system," *IEEE Transactions on Robotics*, 2025.
 - [65] T. Jin, X. Xu, Y. Yang, S. Yuan, T.-M. Nguyen, J. Li, and L. Xie, "Robust loop closure by textual cues in challenging environments," *IEEE Robotics and Automation Letters*, 2024.
 - [66] J. Li, Z. Liu, X. Xu, J. Liu, S. Yuan, and L. Xie, "Limo-calib: On-site fast lidar-motor calibration for quadruped robot-based panoramic 3d sensing system," *arXiv preprint arXiv:2502.12655*, 2025.
 - [67] J. Xu, G. Huang, W. Yu, X. Zhang, L. Zhao, R. Li, S. Yuan, and L. Xie, "Selective kalman filter: When and how to fuse multi-sensor information to overcome degeneracy in slam," *arXiv preprint arXiv:2412.17235*, 2024.
 - [68] S. Yuan, B. Lou, T.-M. Nguyen, P. Yin, M. Cao, X. Xu, J. Li, J. Xu, S. Chen, and L. Xie, "Large-scale uwb anchor calibration and one-shot localization using gaussian process," in *Proceedings of the 2025 IEEE International Conference on Robotics and Automation (ICRA)*, Atlanta, USA, May 2025.
 - [69] T. Ji, S. Yuan, and L. Xie, "Robust rgb-d slam in dynamic environments for autonomous vehicles," in *Proceedings of the 17th International Conference on Control, Automation, Robotics and Vision (ICARCV)*. Singapore: IEEE, December 2022, pp. 665–671.
 - [70] P. Yin, S. Yuan, H. Cao, X. Ji, S. Zhang, and L. Xie, "Segregator: Global point cloud registration with semantic and geometric cues," in *2023 IEEE International Conference on Robotics and Automation (ICRA)*. IEEE, 2023, pp. 2848–2854.
 - [71] C. Zheng, W. Xu, Z. Zou, T. Hua, C. Yuan, D. He, B. Zhou, Z. Liu, J. Lin, F. Zhu *et al.*, "Fast-livo2: Fast, direct lidar-inertial-visual odometry," *IEEE Transactions on Robotics*, 2024.
 - [72] P. Yin, H. Cao, T.-M. Nguyen, S. Yuan, S. Zhang, K. Liu, and L. Xie, "Outram: One-shot global localization via triangulated scene graph and global outlier pruning," in *2024 IEEE International Conference on Robotics and Automation (ICRA)*. IEEE, 2024, pp. 13 717–13 723.
 - [73] G. Kim and A. Kim, "Scan context: Egocentric spatial descriptor for place recognition within 3d point cloud map," in *2018 IEEE/RSJ International Conference on Intelligent Robots and Systems (IROS)*. IEEE, 2018, pp. 4802–4809.
 - [74] H. Wang, C. Wang, C.-L. Chen, and L. Xie, "F-loam: Fast lidar odometry and mapping," in *2021 IEEE/RSJ International Conference on Intelligent Robots and Systems (IROS)*. IEEE, 2021, pp. 4390–4396.